Nano Research

Flurbiprofen microneedle patches for the management of acute postoperative pain

Huaqing Chu[1,2], Yanyan Zhang[2,3], Yuan Yang[5], Jiangtao Xue[2,4], Cong Li[2], Wei Zhang[3] (✉), Zhou Li[2] (✉), and Hui Zheng[1] (✉)

[1] National Cancer Center/National Clinical Research Center for Cancer/Cancer Hospital, Chinese Academy of Medical Sciences and Peking Union Medical College, Beijing 100021, China

[2] Beijing Institute of Nanoenergy and Nanosystems, Chinese Academy of Sciences, Beijing 101400, China

[3] Key Laboratory of Hunan Province for Integrated Traditional Chinese and Western Medicine on Prevention and Treatment of Cardio-Cerebral Diseases, School of Integrated Chinese and Western Medicine, Hunan University of Chinese Medicine, Changsha 410208, China

[4] School of Life Science, Institute of Engineering Medicine, Beijing Institute of Technology, Beijing 100081, China

[5] Institute of Process Engineering, Chinese Academy of Sciences, Beijing 100190, China

ABSTRACT

Acute postoperative pain is commonly treated with flurbiprofen (FBP), but conventional delivery methods are suboptimal. This study prepared a new non-burst release microneedles (MNs) using genipin cross-linked gelatin (cGel). By adding varying amounts of genipin to modulate the crosslinking degree of cGel, the drug release behavior of the drug-loaded MNs in the skin can be altered. The crosslinking parameters that meet therapeutic requirements are selected, thus providing rapid and long-lasting analgesic effects. cGel solutions were successfully cross-linked, altering matrix material microstructure, confirmed by scanning electron microscope imaging and fourier transform infrared spectroscopy. MNs demonstrated increasing mechanical strength with higher crosslinking. Drug release rates were rapid initially, then slowed, exhibiting a characteristic of decreased release rates with increasing degrees of crosslinking. *In vivo*, FBP/cGel MNs significantly reduced allodynia and hyperalgesia post-surgery, with the greatest effect observed at 2–3 h post-surgery, and can maintain analgesia for up to 6 h. Biosafety tests confirmed good biocompatibility. FBP/cGel MNs effectively penetrate the stratum corneum, safely delivering drugs with significant analgesic effects, excellent mechanical properties, and good biocompatibility, representing a promising strategy for managing acute postoperative pain.

KEYWORDS

microneedle, postoperative pain, flurbiprofen, non-steroid anti-inflammatory drug, cross-linked gelatin

1 Introduction

Acute postoperative pain not only affects patients' early postoperative activities and rehabilitation but also has an impact on their emotional and psychological well-being [1]. Hence, perfect postoperative pain management is of paramount importance [2]. Despite opioids being the analgesics of choice during the perioperative period, their use is often associated with adverse reactions such as respiratory depression, pruritus, nausea, vomiting, and drug dependence [3]. With the dissemination of Enhanced Recovery After Surgery (ERAS) protocols and multimodal analgesic strategies, clinicians often adopt a variety of analgesic drugs and techniques to achieve synergistic pain relief [4, 5]. This approach not only reduces opioid consumption but also alleviates the intensity of pain and the occurrence of adverse reactions. Among these, non-steroidal anti-inflammatory drugs (NSAIDs) such as flurbiprofen (FBP), loxoprofen, and ibuprofen are among the most commonly utilized non-opioid analgesics [6], recognized by the ERAS Society as a component of multimodal analgesic strategies [7]. NSAIDs primarily function through the inhibition of cyclooxygenase activity, suppressing the synthesis of prostaglandins, thereby exerting analgesic and anti-inflammatory effects [8]. They have been extensively applied in the management of perioperative pain, osteoarthritic pain, migraine, and dental pain, among other mild to moderate pain. Research indicates that the application of NSAIDs not only effectively reduces postoperative pain but can also decrease the required doses of opioid medications, thereby lowering the incidence of postoperative nausea and vomiting [9].

FBP, a clinically prevalent NSAID, shares the aforementioned characteristics of NSAIDs. Administration routes for FBP include intravenous injection of flurbiprofen axetil, the prodrug of flurbiprofen, and transdermal delivery via FBP hydrogel patch (HP) [10, 11]. However, both modes of administration exhibit distinct disadvantages. Intravenous injection necessitates the proficiency and experience of a trained operator. Concurrently, a temporal delay between the onset of patient pain and the execution of medical orders is present. Due to the lack of patient self-control, intravenous injections struggle to promptly address acute pain episodes, potentially resulting in suboptimal healthcare experiences and heightened pain apprehension for the patient.

Additionally, intravenous injections carry risks such as injection pain, needle phobia, local infections, and even the potential for nerve damage [12, 13]. While HP offers improved patient compliance due to their non-invasive nature, the efficiency of transdermal drug delivery is often compromised by the barrier function of the stratum corneum [14]. In recent years, research has focused on enhancing the transdermal delivery of HP through the use of chemical penetration enhancers or pharmacological techniques, such as employing nanocarriers to encapsulate drugs. However, while these chemical enhancers can increase transdermal absorption rates to a certain extent, their effectiveness is often limited [15, 16]. Therefore, there is an urgent need to develop an ideal drug delivery carrier that exhibits excellent patient compliance, is easy to prepare, safe and efficient, with minimal adverse reactions.

Microneedles (MNs) technology, as a novel transdermal drug delivery method, is a physical permeation-enhancing techniques [17]. The MNs array, composed of numerous uniform and neatly arranged micrometer-scale fine needles, possesses outstanding mechanical properties, enabling it to penetrate the stratum corneum and deliver the encapsulated drug to the deeper layers of the skin [18]. MNs effectively compensate for the shortcomings of traditional injection needles and transdermal patches, offering advantages such as minimally invasive, painless, avoidance of first-pass metabolism, localized delivery, and self-administration [19, 20]. The matrix materials used for fabricating MNs are diverse, including metals [21], silicon [22], ceramics [23], and polymers [24, 25]. MNs made from polymer materials are widely used in research for controlled drug release and sustained drug release [26, 27]. They offer several advantages, including the ready availability of materials, safety and non-toxicity, solubility, biodegradability, simple manufacturing processes, and the potential for mass production. These features make polymer-based MNs a promising tool for the future of drug delivery systems. Gelatin (Gel), derived from animal collagen and approved by the Food and Drug Administration (FDA) as a natural medical polymer material, offers various advantages such as its wide availability, rich content, and good biocompatibility. These properties make Gel a common choice in drug delivery, tissue repair, and other biomedical applications [28, 29]. However, Gel has weak mechanical properties, and the MNs produced from it exhibit inferior mechanical performance. Moreover, due to its strong hydrophilicity that allows for quick dissolution, drug-loaded MNs prepared from Gel are prone to burst release, making them more suitable for applications requiring rapid and short-term drug delivery. Physical or chemical crosslinking can alter the internal forces or the intermolecular network structure of natural gelatin, significantly enhancing its mechanical properties [30]. Commonly used crosslinking agents include glutaraldehyde, genipin, and diisocyanates [31, 32]. Compared to other crosslinking agents, genipin, as a natural biological crosslinker, can undergo chemical crosslinking reactions with Gel under mild conditions, has lower cytotoxicity, and the crosslinking significantly enhances the mechanical properties of cross-linked gelatin (cGel) [33, 34].

In this study, Gel was used as the raw material and genipin as the crosslinking agent to prepare cGel solutions with crosslinking degrees of 9.17%, 24.65%, and 32.71%. These solutions served as the matrix materials for the fabrication of FBP MNs. Utilizing micromolding techniques, drug-loaded MNs patches (MNP) with varied degrees of cross-linking were fabricated. The mechanical properties of MNs progressively increased with the degree of crosslinking. The cumulative drug release rate gradually increased over time, with a faster release rate in the initial phase and a slowdown in the later phase. Moreover, the drug release behavior of the drug-loaded MNP with different crosslinking degrees varied, showing a characteristic of slower release rates with the

increase in crosslinking degree. *In vivo* efficacy evaluation experiments revealed that FBP/cGel MNP could significantly and rapidly alleviate postoperative allodynia and hyperalgesia, with the most pronounced effects occurring 2–3 h after surgery, and could maintain analgesia for approximately 6 h. The skin repair experiments, cytotoxicity tests, and hemolysis tests all demonstrated that the matrix materials selected for this study possessed excellent biocompatibility.

2 Results and discussion

2.1 Synthesis and characterization of MNs matrix material

As shown in Fig. 1(a), this study chemically crosslinked Gel materials using the natural crosslinker genipin, whose multiple active functional groups can react chemically with the amino groups in Gel [35]. The schematic diagram of the principle of genipin crosslinking Gel is shown in Fig. S1 in the Electronic Supplementary Material (ESM), where crosslinking reactions can occur both with-in Gel molecules (short-range intermolecular crosslinking) and between molecules (long-range intermolecular crosslinking), thereby increasing the connections between Gel molecules [30]. After genipin is added to the Gel solution, the solution gradually changes from bright yellow to deep blue, and the color of the solution deepens progressively with the increase in crosslinking time (Fig. S2 in the ESM). As shown in Fig. 1(b), with the increase in adding genipin, the color of the cGel solution becomes darker and the viscosity increases. When the amount of genipin added reaches 300 µL, the fluidity of the solution significantly deteriorates, rendering it unsuitable for the preparation of drug-loaded MNs using the template filling method. Scanning electron microscope (SEM) observations of the material's microstructure, as presented in Fig. 1(b), reveal that Gel exhibits a loosely porous structure with irregularly sized and distributed pores. After crosslinking with genipin, the material forms a compact, porous, and well-interconnected spatial network structure. As the crosslinking agent con-centration increases, the pore size within the network decreases and the number of pores increases.

As depicted in Fig. 1(c), there are distinct differences between the Fourier transform infrared spectroscopy (FT-IR) of Gel and cGel, indicating structural changes in the Gel material during the crosslinking reaction. Compared to the FT-IR of Gel, the N–H band of cGel shifts toward a lower wave-number (from 1245 to 1240 cm^{-1}), which strongly suggests the involvement of N–H groups in hydrogen bond formation, signifying that a chemical crosslinking reaction has occurred between the amino groups of Gel and genipin.

In this study, the ninhydrin method was utilized to determine the concentration of glycine standard solutions across a series of gradients, which were then used to plot a standard curve and derive a linear regression equation, $Y = 1.129 \cdot X - 0.02665$, with an $R^2 = 0.9930$ (Fig. 1(d)). Using the same testing method, the crosslinking degrees of cGel prepared with 100, 200, and 300 µL of genipin were measured to be 9.17%, 24.65%, and 32.71%, respectively (Fig. 1(e)).

2.2 Preparation and morphology characterization of MNs

Figure 2(a) illustrates the process schematic for fabricating drug-loaded MNs using the mold casting technique. The drug-loaded cGel, crosslinked with genipin, serves as the matrix material for the MNs, while the cGel without any drug is utilized as the backing layer.

According to Fig. 2(b), the study successfully fabricated a 10 ×
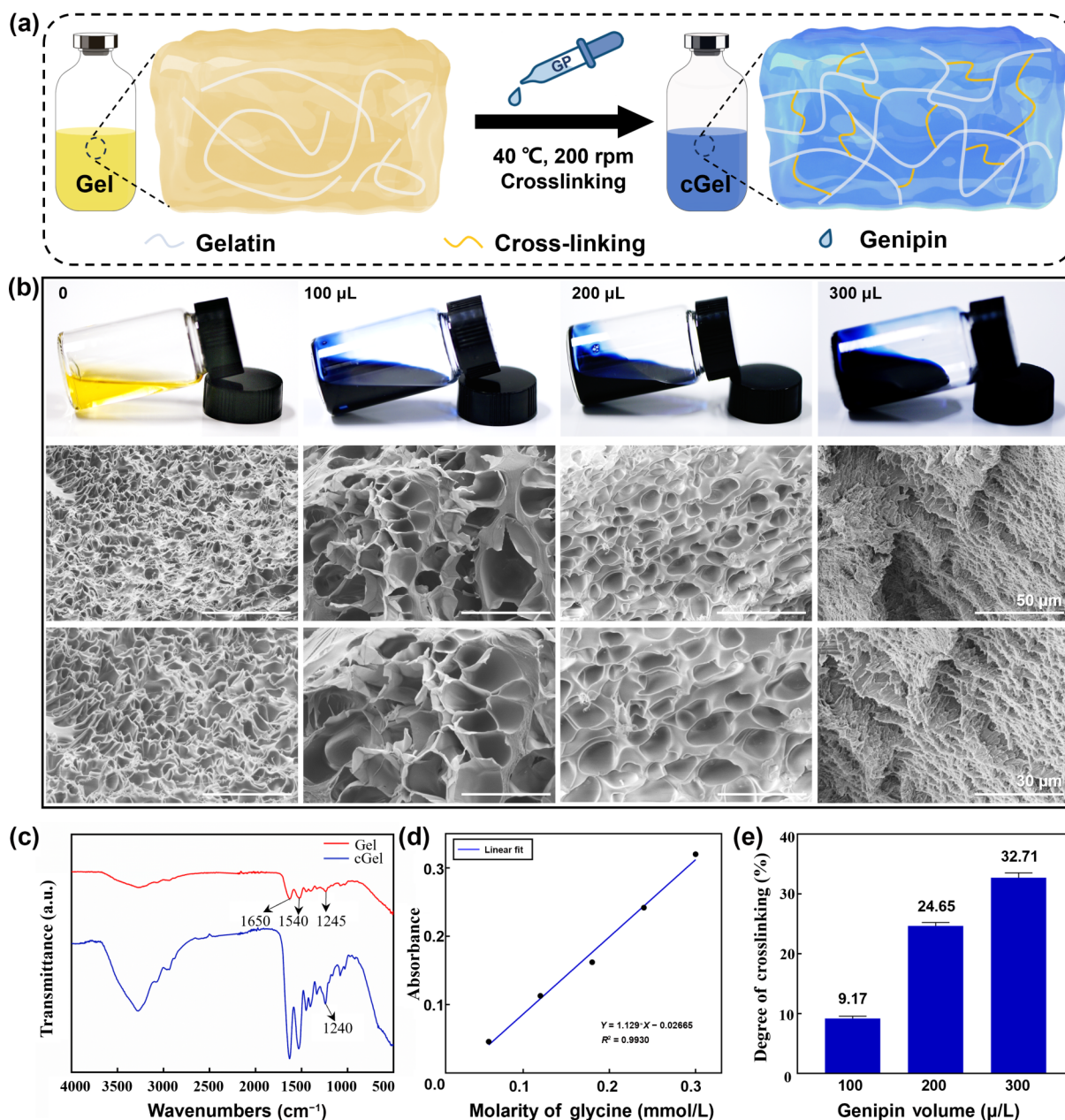
Figure 1 Synthesis and characterization of MNs matrix materials. (a) Preparation of cGel solutions. (b) Schematic representations of cGel solutions with varying crosslinking degrees and their microstructures as observed under a SEM. (c) FT-IR of Gel and cGel. The crosslinking degree of cGel was determined by the Ninhydrin method, with the glycine standard curve shown in (d) and the crosslinking degree of cGel adding various volume genipin presented in (e) ($n = 5$).

10 array of cGel MNs, with the entire array measuring approximately 4.8 mm by 4.8 mm. The MNs array is intact, with sharp tips and no bending, breaking, or missing needles observed. The needles are conical, with a height of about 650 μm, a needle spacing of 500 μm, and a base diameter of 300 μm. Figure S3 in the ESM provides a bright field schematic view of the Gel MNs. The SEM schematic provides a clear view of the drug-loaded cGel MNs from both lateral and top perspectives, showcasing the microsurface of the MNs. The tips of the MNs are intact, and the surface of the needle body is smooth, with no roughness or drug precipitation observed on the surface of the needles. This observation indicates a successful incorporation of the drug into the cGel matrix, ensuring that the drug is evenly distributed within the microneedles without affecting the structural integrity and surface smoothness of the MNs.

2.3 Mechanical and insertion properties of FBP/cGel MNs

Figure 3(a) presents the schematic of the axial force testing method for FBP/cGel MNs and the results of the force–displacement curves. As the force applied to the MNs increases, the displacement of the needle tip also increases, but there is never a sudden drop in force (i.e., no appearance of breakpoint force). This suggests that the increase in pressure applied to the MNs during axial force testing does not cause the FBP/cGel MNs to fracture, but merely results in bending deformation. Under an optical microscope, the morphological changes experienced by the FBP/cGel MNs before (Fig. S4(a) in the ESM) and after (Fig. S4(b) in the ESM) the axial force tests are more intuitively presented. After the Mark-10 test, the needle tips are bent, but there is no fracture or breakage of the needle bodies, which is consistent with the above-mentioned results of the force–displacement curves obtained from the axial force tests. The results from the force–displacement curves suggest that with the increase in adding genipin, the mechanical properties of FBP/cGel MNs are progressively enhanced (i.e., the mechanical strength is in the order of: cGel-300 MNs > cGel-200 MNs > cGel-100 MNs > Gel MNs). This can be attributed to the fact that with the increase in
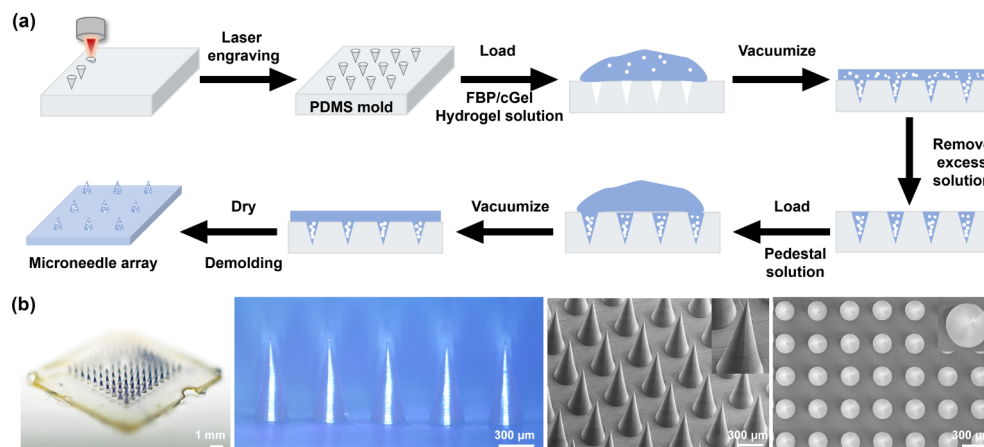
Figure 2 (a) Flowchart of the preparation method for FBP/cGel MNs. (b) Morphology of the FBP/cGel MNs imaged by metallographic microscope and SEM.
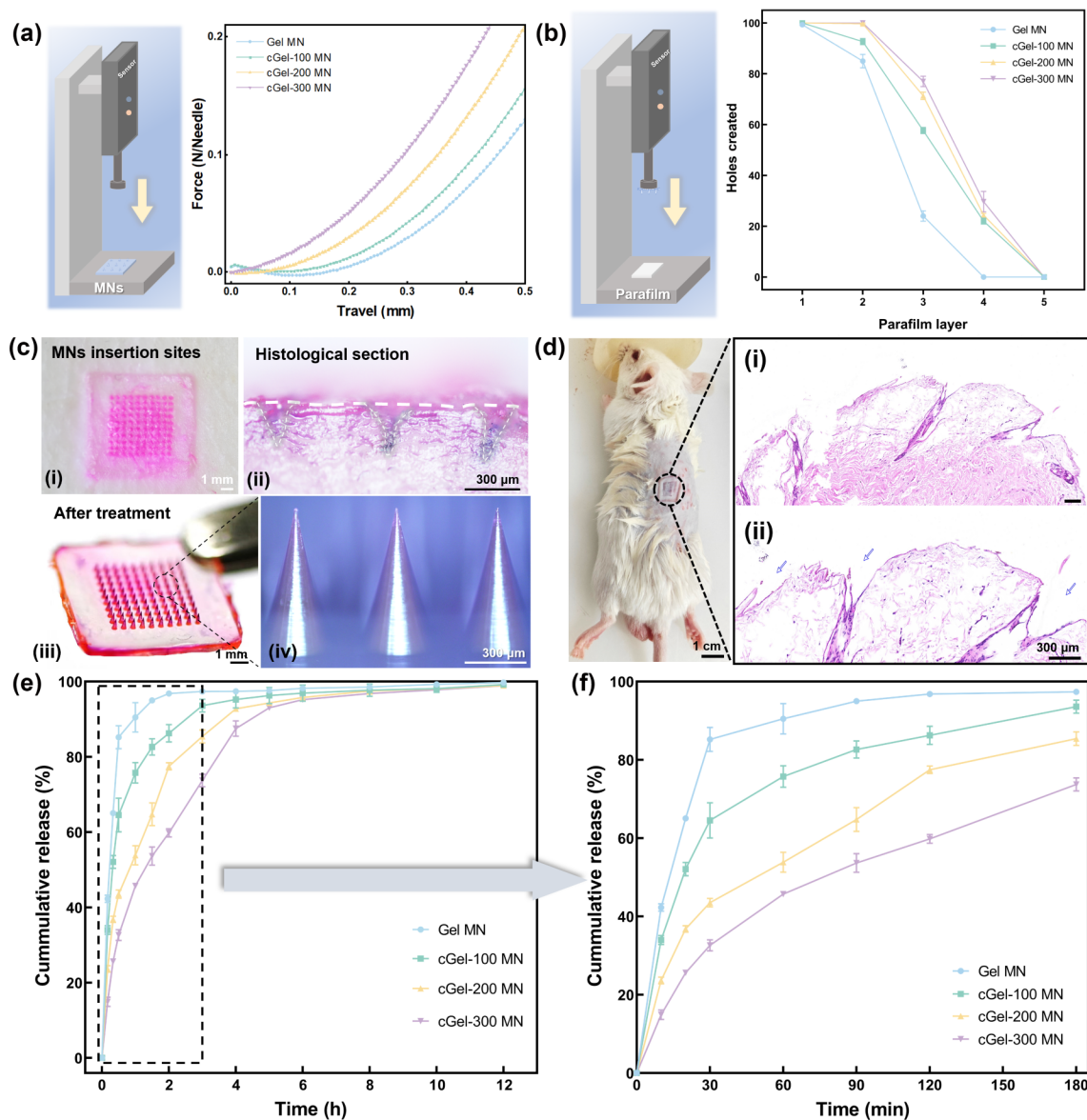
Figure 3 (a) Schematic diagram of the axial force test method and the force–displacement curves for each group of FBP MNs. (b) Test method for the FBP MNs penetration into the sealing film and the penetration layers–hole count curves for each group of FBP MNs ($n = 3$). (c) Inserting porcine skin experiment with RhB/cGel MNs. ((i) Schematic illustration of the needle holes on the porcine skin surface after MNs removal. (ii) Schematic illustration of the vertical cross-section of the microchannels created by MNs penetration into porcine skin. (iii) Schematic illustration of the MNs morphology after removing from porcine skin. (iv) Schematic illustration of the localized magnification of the MNs after removal). (d) Mouse skin penetration experiment with FBP/cGel MNs. Left image: penetration of FBP/cGel MNs into the back of an anesthetized Kunming mouse. Right image: localized HE-stained section of mouse back skin after penetration with FBP/cGel MNs, where the blue arrows indicate the microchannels created by the MNs. (e) *In vitro* cumulative drug release curves of different crosslinked FBP MNs groups ($n = 5$). (f) Cumulative drug release curves for the first 3 h ($n = 5$).

crosslinking degree, the internal network structure of cGel becomes more stable and denser [36]. This is supported at the microscopic structural level by the SEM in Fig. 1(b).

As shown in Fig. 3(b), the method and result of piercing the sealing film with FBP MNs are illustrated. It can be seen that the piercing performance of the cGel MNs group on the sealing film is superior to that of the Gel MNs group. Observing the Parafilm M® film of each group, the perforation rate of the four groups of FBP MNs in the first layer of films was almost 100%. In the second layer of films, the perforation rate of the cGel-300 MNs group and the cGel-200 MNs group remained at 100%. However, the perforation rates of the Gel MNs group and the cGel-100 MNs group began to decrease from the second layer, especially the Gel MNs group, which had a perforation rate of only 24% in the third layer, and the rate dropped to 0 in the fourth layer. The cGel-300 MNs group and the cGel-200 MNs group have nearly similar penetration rates and can both penetrate through four layers of film with penetration rates of approximately 29% and 24% respectively in the fourth layer, suggests that these MNs retain a consistent ability to pierce through multiple layers. According to the Fig. 3(c), after the Rhodamine B (RhB)/cGel MNs were removed from the pigskin, 100 red holes were observed on the surface of the pigskin. The red coloration, which comes from the RhB, indicates that the drug has been effectively delivered into the pigskin, as the color did not wipe off. Additionally, microscopic observation revealed that the depth of the holes was around 300 μm, which is indeed sufficient to penetrate the stratum corneum (about 10–20 μm). Besides, the RhB/cGel MNs remain intact after being removed from the skin—with no dissolution or breakage—indicates that the MNs are robust enough to withstand insertion into and retraction from the skin without losing their structural integrity. Additionally, as demonstrated in Fig. 3(d), FBP/cGel MNs also effectively penetrated the skin.

2.4 Drug release behavior of FBP/cGel MNs

To quantitatively determine the drug release behavior of FBP/cGel MNs, this study enclosed the FBP MNs of each group in sealed bags containing release medium (phosphate buffer saline (PBS) with 10% ethanol), and maintained them in a beaker at 37 °C and 300 rpm for continuous drug release, sampling and testing at corresponding time points. After 12 h, the FBP MNP were completely dissolved, and the drug release at this time was considered to be the total drug load of the MNs. Finally, the cumulative drug release rate of MNs from each group at various time points was calculated to clarify the drug release process of the MNs.

Figure S5(a) in the ESM presents the molecular structure of FBP, which has a molecular weight of 244.26 Dalton (Da). In this study, the molecular weight of the matrix materials used to fabricate MNs is greater than 1000 Da; therefore, dialysis bags with a molecular weight cut-off (MWCO) of 1000 Da were chosen for the drug release experiments. As depicted in Fig. S5(b) in the ESM, the study determined the optical density (OD) values at 247 nm for FBP standard solutions of concentrations 1, 2, 4, 6, and 8 μg/mL, and plotted a standard curve to obtain the linear regression equation, $Y = 0.0857 \cdot X - 0.0262$, $R^2 = 0.9931$.

As shown in Figs. 3(e) and 3(f), the cumulative release rate of FBP gradually increased with the extension of release time. Each group exhibited a rapid release rate in the early stages of drug release, which slowed down in the later stages. The Gel MNs group reached a cumulative drug release rate of over 90% in the first hour, while the cGel-100 MNs, cGel-200 MNs, and cGel-300 MNs groups achieved cumulative drug release rates of 76%, 54%, and 46% in the first hour, respectively. The drug release behavior of FBP MNs with different degrees of crosslinking varies, generally showing a trend where the release rate slows down as the degree of crosslinking increases. The four groups of FBP MNs took approximately 0.5, 1.5, 3, and 4 h, respectively, to reach a cumulative drug release of about 80% or more. These characteristics indicate that upon application to the skin environment, FBP MNs absorb moisture from the surrounding tissue and swell gradually; the rate at which the small drug molecules diffuse from the spatial network into the tissue is closely related to the microscopic structure of the matrix material.
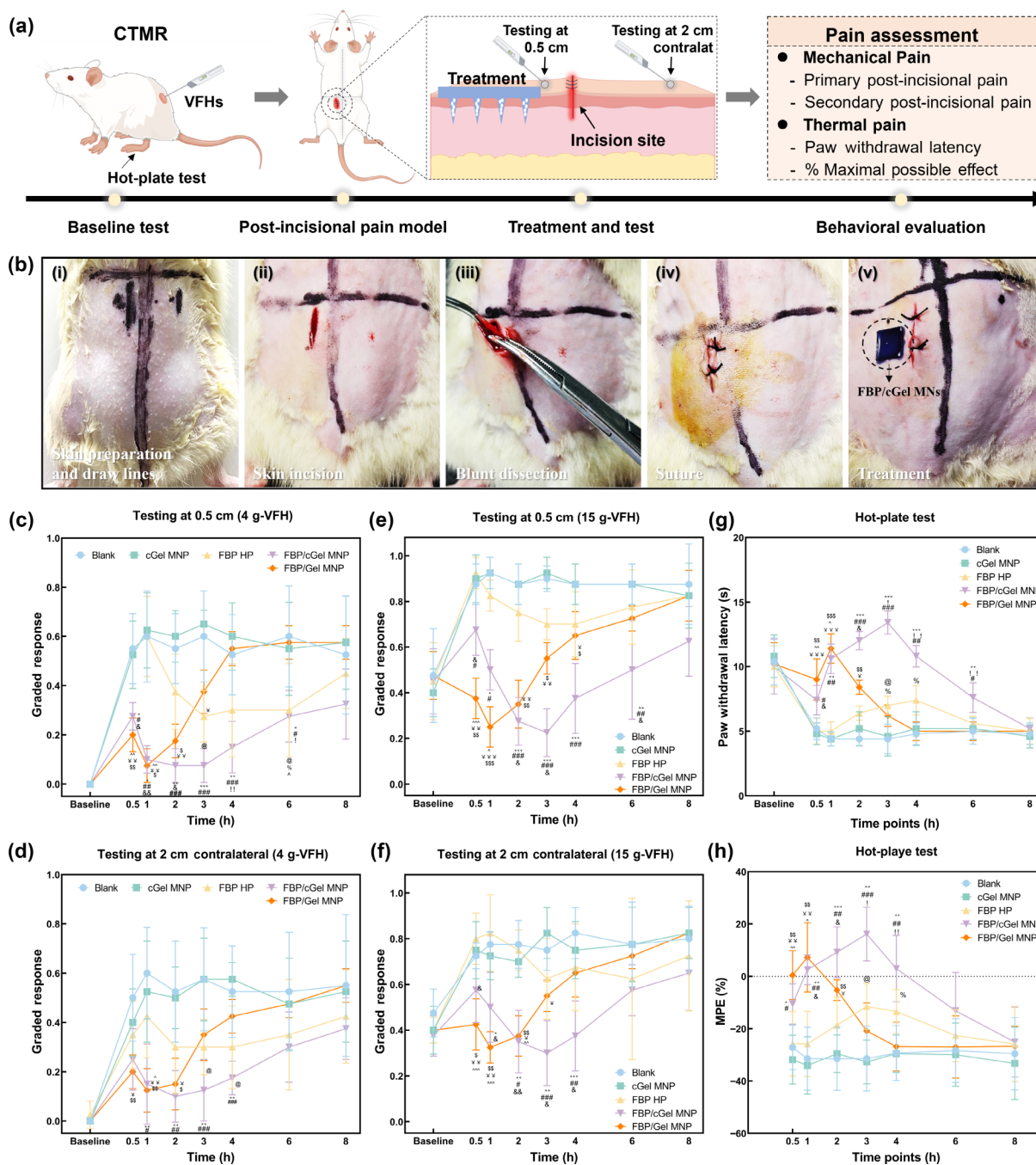
2.5 Analgesic efficacy of MNs

Considering the preparation conditions, morphological characterization, mechanical property testing, and drug release behavior of the FBP MNs, and taking into account the clinical requirements for the release kinetics and analgesic duration of the pain relief medication (rapid onset and sustained action), we chose FBP/cGel-200 MNs as the MNs preparation parameters for the *in vivo* analgesic effect study.

Figure 4(a) is the experimental design roadmap for the efficacy study. As shown in Fig. 4(b), this study adopted the modified rat dorsal hairy skin incision pain model by Ohri et al. [37]. Following the completion of modeling and treatment, behavioral tests were conducted on rats from each group using mechanical and thermal pain stimuli.

Different thicknesses of von Frey hairs (VFHs) were used to stimulate the skin at various distances from the rat's incision to observe changes in the cutaneous trunci muscle reflex (CTMR) to assess the local and systemic analgesic effects of FBP/cGel MNs. Before modeling, baseline measurements were taken at 0.5 cm on the same side (primary pain sensitization) and 2 cm on the contralateral side (secondary pain sensitization) of the planned surgical incision in all healthy rats using 4 g- and 15 g-VFHs. Since all rats were subjected to habituation stimuli preoperatively, there was no response to the 4 g-VFH (non-noxious stimulus) test in all rats (Figs. 4(c)–4(f)). However, Figs. 4(g) and 4(h) indicate that the baseline value for the 15 g-VFH was approximately 0.44 ± 0.027, showing that healthy rats had a significant response to the 15 g-VFH.

The increases in response to both the 4 g- and 15 g-VFHs at 0.5 cm on the ipsilateral side and 2 cm on the contralateral side in all groups of rats half an hour after treatment suggests that the rats experienced an increased sensitivity to stimuli in the areas surrounding the incision (primary sensitization) as well as in areas further away from the incision (secondary sensitization), which are typical signs of sensitization after tissue injury. During the subsequent 8 h testing period, rats from both the Blank group and the cGel MNP group continued to display high response levels to 4 g- and 15 g-VFHs. As depicted in Figs. 4(c) and 4(d), primary and secondary allodynia responses in the FBP/cGel MNP group were significantly alleviated from 30 min to 6 h post-surgery, with the most pronounced effect observed at 2 h post-surgery (graded response score of 0.075 ± 0.061 at 0.5 cm ipsilateral and 0.100 ± 0.093 contralateral to the 4 g-VFH). Additionally, the FBP/cGel MNP group exhibited more pronounced and prolonged alleviation of primary allodynia compared to secondary allodynia, as can be more vividly illustrated through the population response outcomes (Figs. S6(a) and S6(b) in the ESM). The alleviation of hyperalgesia in rats treated with FBP/cGel MNP was analogous to the mitigation of allodynia. Compared to the Blank group and the cGel MNP group, from 30 min to 6 h post-surgery, the FBP/cGel MNP group exhibited a significant improvement in primary hyperalgesia. Likewise, from 1 to 4 h post-surgery, FBP/cGel MNP also significantly ameliorated secondary hyperalgesia in rats. Analysis revealed that at 3 h post-surgery, both primary and secondary hyperalgesia in the FBP/cGel MNP group were most

Figure 4 Analgesic efficacy study (n = 5). (a) Experimental design roadmap for efficacy evaluation. (b) Flowchart for the method of constructing a rat dorsal hairy skin incision pain model. (c)–(h) Evaluation of analgesic effects on mechanical pain in rats. Graded response of primary (c) and secondary (d) allodynia across groups. Graded response of primary (e) and secondary (f) hyperalgesia across groups. In the hot-plate test, the hind PWL (g) and %MPE (h) were measured for each group of rats.

substantially alleviated (with a graded response score of 0.225 ± 0.093 at 0.5 cm ipsilateral and 0.300 ± 0.127 at 2 cm contralateral to the 15 g-VFH). In addition, as observed in Figs. 4(c)–4(f), the FBP/Gel MNP group demonstrated a rapid onset of analgesic effect within half an hour post-surgery, reaching its peak analgesic efficacy at one hour post-surgery. However, the analgesic effect was transient, with the average duration of action lasting only 3–4 h post-surgery. This suggests that due to the rapid release of the drug by FBP/Gel MNP, it produces a quick yet short-lived analgesic effect, making it more suitable for the treatment of acute breakthrough pain. Furthermore, there was no statistically significant difference in the graded response scores between the FBP/Gel MNP group and the FBP/cGel MNP group (P > 0.05). The FBP/Gel MNP did not exhibit a more potent analgesic effect despite the rapid release of a large amount of FBP, which may be

attributed to the ceiling effect of FBP. Crucially, an analysis of the result curves for the FBP HP group revealed that the stimulus response in the rats of this group was also alleviated to some extent, but the analgesic effect was slow to onset, modest in degree, and short-lived. Compared with the Blank group and the cGel MNP group, in most cases, the improvement on pain sensitization in the FBP HP group was not statistically significant (P > 0.05).

The response of rats in each group to thermal pain stimuli was evaluated using the hot-plate test. By recording the hind paw withdrawal latency (PWL) of rats in each group, the changes in thermal pain threshold were reflected. The anti-nociceptive effect of each group was then expressed as a percentage of the maximum possible effect (%MPE). As shown in Figs. 4(g) and 4(h), the PWL of rats in all groups initially decreased postoperatively, which was attributed to the stress caused by surgery and the formation of

pain sensitization. Similar to the results observed with mechanical stimuli, the rats in the FBP/cGel MNP group experienced significant relief from thermal pain between 1 and 4 h post-surgery, with a rapid onset and sustained effect. The rats in the FBP/Gel MNP group had temporary relief from thermal pain between 0.5 and 1 h post-surgery. The PWL of the other three groups after surgery was shorter than the baseline PWL, indicating that the treatments in these three groups were ineffective in alleviating thermal pain stimuli.

2.6 Biocompatibility of FBP/cGel MNs

As shown in Fig. 5(a), the skin recovery in the area treated with MNPs was observed every 1 h. Over time, the skin visibly healed with the red drug gradually being absorbed and fading. At 3 h post-treatment, the skin was almost completely healed with no signs of infection, skin lesions, or permanent damage. This rapid skin recovery and drug absorption process demonstrate the minimally invasive nature of the MNs and the good biocompatibility of the matrix material used in this study.

According to ISO 10993-5 standards, a material is considered to have no or low cyto-toxicity when the relative cell viability after incubation with the material is greater than 80% (grade 0 or 1 cytotoxicity) [38]. As illustrated in Figs. 5(b)–5(d), L-929 cells incubated for 24 h with various concentrations of Gel solution (Fig. 5(b)), FBP solution (Fig. 5(c)), and FBP/cGel MNs extract (Fig. 5(d)) showed relative cell viabilities well above 80%. This indicates that the drug delivery system possesses low cytotoxicity. The low cytotoxicity can be attributed to the use of the natural cross-linking agent genipin, which is less toxic and used in small quantities, and Gel, which is a non-toxic natural polymer material.

According to ISO 10993-4 and ASTM F 756-00 standards, a sample is considered to have good hemocompatibility if the average hemolysis rate of repeated trials is less than 5% [39]. As indicated in Fig. 5(e), the average hemolysis rates for cGel MNs and FBP/cGel MNs were 0.164% and 0.779%, respectively, both significantly below the 5% criterion. Furthermore, observation of erythrocyte morphology under optical microscopy showed complete rupture of red blood cells with ultrapure water as the positive control. In contrast, red blood cells treated with cGel MNs and FBP/cGel MNs extracts, similar to those with PBS as the negative control, exhibited no significant difference, maintaining a disc-shaped morphology without evident rupture. This also demonstrates the system's good hemocompatibility.

3 Conclusions

In summary, this study developed a transdermal drug delivery system, FBP/cGel MNs, for postoperative pain management. By adjusting the amount of the cross-linking agent genipin, the cross-linking degree and microstructure of the MNs matrix material were altered to regulate the drug release behavior of the FBP/cGel MNs. Combined with material and MNs morphology characterization, mechanical performance testing, and biocompatibility evaluation, this drug-loaded MNP can effectively and safely perform transdermal drug delivery. Unlike the classic plantar incision pain model, the hairy skin incision pain model on the rat back more accurately simulates the therapeutic effect on postoperative pain in patients. Behavioral results in animals suggest that compared with FBP HP and FBP/Gel MNP, FBP/cGel MNP can rapidly exert an analgesic effect (in about half an hour) without burst release, maintaining a relatively long-lasting analgesic effect (about 6 h). The FBP/cGel MNP designed in this study are simple to prepare, with excellent mechanical properties, significant analgesic effects, and good biosafety. This

MNP provides an effective new strategy for treating postoperative pain in patients and has good clinical application value.

4 Materials and methods

4.1 Materials

Polydimethylsiloxane (PDMS, Sylgard 184) was obtained from Dow Corning (Midland, USA). Gel (from cold water fish skin, $M_W \approx 60,000$ Da), FBP, PBS, and sodium acetate-acetic acid buffe (pH 5.4) were purchased from Sigma-Aldrich (MO, USA). Cell counting kit-8 (CCK-8), tissue cell fixative solution (4%), and Rhodamine B (RhB) were purchased from Beijing Solarbio Science & Technology Co., Ltd. (Beijing, China). Genipin was purchased from Macklin Biochemical Co., Ltd. (Shanghai, China). Potassium bromide (KBr), glycine, and HE staining kits were purchased from Aladdin Biochemical Technology Co., Ltd. (Shanghai, China). Mouse fibroblast cell lines (L-929 cells) were purchased from iCell Bioscience (Shanghai, China), and female Sprague-Dawley (SD) rats, male Kunming mice, and New Zealand Rabbits were obtained from the Institute of Laboratory Animal Sciences (Beijing, China). Ninhydrin was purchased from J & K Scientific (Beijing, China).

4.2 Synthesis and characterization of MNs matrix materials

According to the method reported by Chen et al. [40], drug-loaded and non-drug-loaded cGel solutions were prepared by a blending cross-linking method. Specifically, 8 g of Gel powder was weighed and added to 16 mL of ultrapure water. After sufficient swelling, the mixture was stirred at 50 °C and 300 rpm for 2 h to obtain a 40 w/v% Gel solution. The solution was then left to stand for the removal of air bubbles before being sealed for later use. 20 mg of genipin powder was weighed out and added to 1 mL of a solution containing 10% ethanol. Heat at 40 °C for 2 min, then vortex to facilitate dissolution. 100, 200, and 300 μL of the genipin solution were transfered, respectively, by slowly adding dropwise to the previously prepared 10 g Gel solution. The mixtures were then continuously stirred at 40 °C and 200 rpm for 3 days to allow full cross-linking reactions to occur, ultimately yielding cGels of three different degrees of cross-linking, to be used as backing layer materials for MNs. 50 mg of FBP was weighed and dissolved in 1 mL of a 10% ethanol solution, ensuring the mixture was thoroughly mixed. After that, 200 μL of the Gel solution was took and added an equal volume of the prepared drug solution, stirring well to ensure uniformity. Subsequently, different volumes of the genipin solution were added to perform cross-linking, obtaining drug-loaded cGel solutions with varying degrees of cross-linking. These solutions served as matrix materials for the preparation of drug-loaded MNs.

FT-IR (VERTEX80v, Bruck, Germany) was utilized to analyze the molecular structure of the MNs matrix materials prepared as mentioned above. Changes in characteristic peaks within the FT-IR spectra were observed to determine the alterations in molecular structure before and after material cross-linking. The MNs matrix materials were lyophilized and sputter-coated with gold, then the microstructural features of the materials were observed under a SEM (SU8020, Hitachi, Japan).

This study employed the ninhydrin reaction to determine the changes in amino acid content before and after cross-linking, thereby measuring the degree of cross-linking [41]. Aliquot 0, 0.2, 0.4, 0.6, 0.8, and 1 mL of a 0.3 mmol/L standard glycine solution into sample vials and make up to 1 mL with ultrapure water respectively. Subsequently, add 1 mL of acetate buffer (pH 5.4, 2 mol/L) and 1 mL of ninhydrin reagent to each vial, mix thoroughly, and heat in a boiling water bath for 15 min.
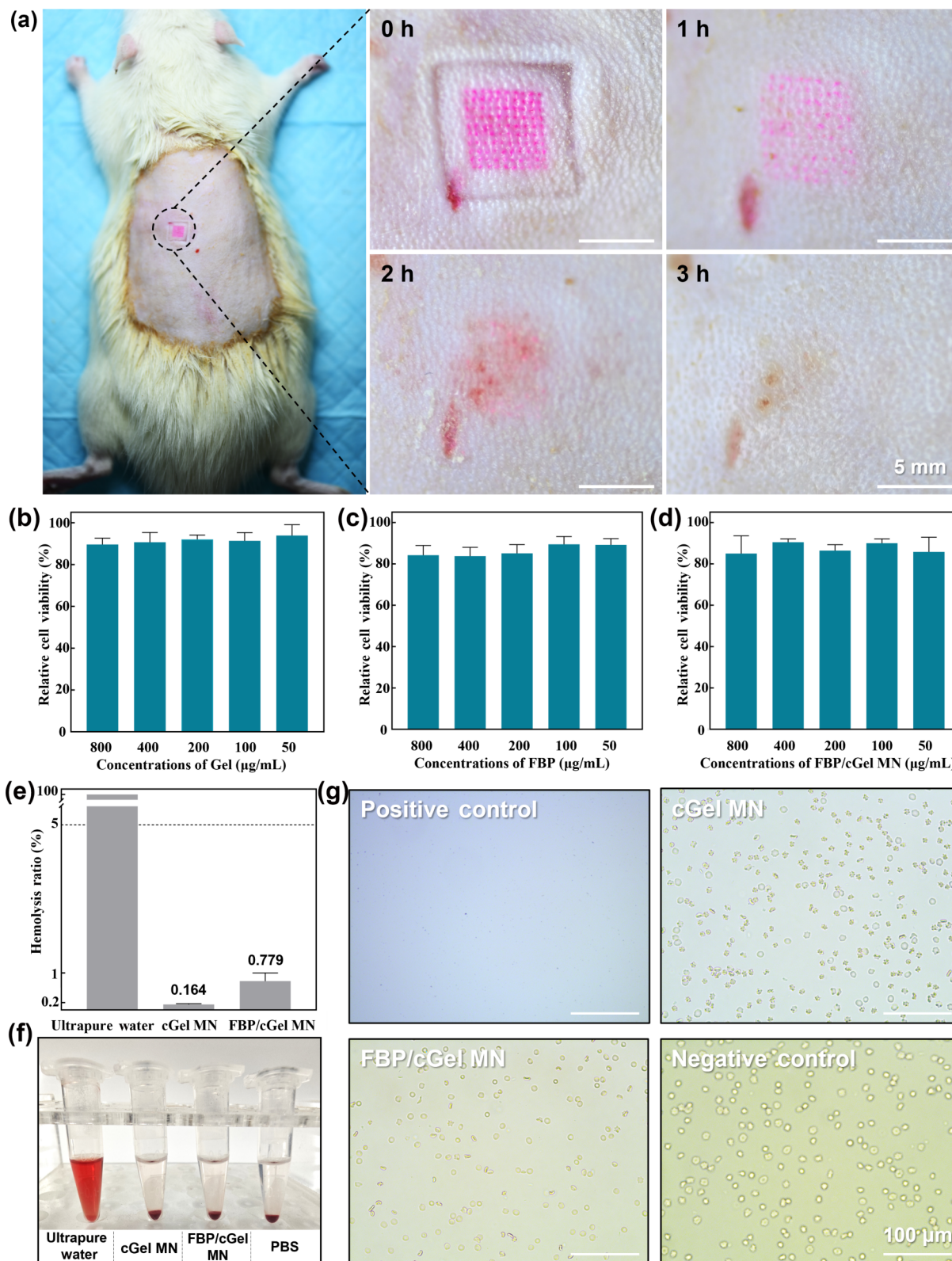
Figure 5 Biocompatibility assessment. (a) Schematic of skin recovery in rats post-application of RhB/cGel MNP on dorsal skin. (b)–(d) Cytotoxicity test. Relative viability of L-929 cells after incubation with various concentrations of Gel solution (b), FBP solution (c), and FBP/cGel MNP extracts (d). (e)–(g) Hemolysis test. Hemolysis rate (e) and hemolytic phenomena (f) after incubation of erythrocytes with different solutions. (g) Morphology of erythrocytes from each group under optical microscopy.

Immediately cool with tap water and let stand for 5 min. Then, add 3 mL of 60% ethanol solution for dilution and shake well. Lastly, measure the absorbance at a wavelength of 570 nm using a multifunctional microplate reader (Varioskan™ LUX, Thermo Fisher TM), obtain the linear regression equation, and plot the standard curve. Using the same operational procedure as above, measure the absorbance of the sample solution at 570 nm.

Calculate the crosslinking degree of each sample using the following Eq. (1)

$$\text{Modified degrees } (\%) = (M_o - M_c)/M_o \times 100\% \qquad (1)$$

where M_o represents the amino groups content in Gel, and M_c is the amino groups content in cGel.

4.3 Fabrication and morphology characterization of MNs

Micromolding was used to fabricate drug-loaded MNs, and PDMS molds were prepared according to the method described by Wang et al [42]. The MNs matrix solution was filled into the mold cavities by applying vacuum to the bottom of the PDMS molds using a vacuum setup. A 200 μL volume of the drug-loaded cGel MNs matrix solution (FBP/cGel or RhB/cGel) was evenly dropped onto the PDMS mold, followed by negative pressure suction for 45 min until the material solution filled the mold cavities. Subsequently, a plastic scraper of appropriate size was used to remove the excess matrix solution on the top layer. Subsequently, 200 μL of the non-drug cGel solution was coated on the PDMS mold, followed by another 10 min of vacuum suction to form the backing layer of the MNs. Finally, the vacuumed PDMS mold was placed in a fume hood to dry and solidify overnight naturally. Once thoroughly dried, the mold was demolded, and the prepared MNs were transferred to a vacuum drying oven for storage to ensure they remain dry.

Employing metallographic microscopy (ECLIPSE, Nikon) and SEM, observe the surface morphology of MNs to ascertain if the fabricated MNs meet the required standards, including the presence of needle fractures, uneven drug loading, and other related issues.

4.4 Mechanical and insertion properties of MNs

Axial force tests, sealing film perforation tests, porcine skin insertion tests, and small animal *in vivo* skin insertion tests on drug-loaded MNs were comprehensively conducted to verify their mechanical properties.

Fully dried MNs are fixed at the center of the tensile and compressive force tester (EMS301, Mark-10, USA) platform, with a Mark-10 descent speed set to 5 mm/min and a stop condition of a compressive load of 20 N. Upon initiation of the test, the software automatically records data pertaining to axial force and tip displacement, saving this for analysis of each test group and for the plotting of force–displacement curves. The morphology of the MNs before and after testing was characterized and recorded using a metallographic microscope to determine if the MNs had fractured or bent after the tests.

Place eight layers of sealing film (Parafilm M®, USA) in the center of the test platform, with the base of the MNs fixed to the probe of the Mark-10. Set the same parameters for the Mark-10. Once reaching 20 N, hold the probe in place for 30 s before lifting and separating the MNs from the sealing film. Count the number of holes in each layer of film and compare the puncture rates of the sealing film by different MNs groups.

Place the RhB/cGel MNs vertically into the pre-treated fresh porcine skin (hairless) for 1 min before removing the MNs. Using a sharp blade to longitudinally slice the porcine skin, observe the depth of the MNs channels from the side, and capture images of the microstructure of the MNs after removal.

Kunming mice skin was used to simulate human skin. The hair on the dorsal skin of the mice was removed, and RhB/cGel MNs were inserted vertically into the mouse skin for 1 min before the MNs were removed. The skin tissue treated with MNs was placed in 4% tissue fixative for fixation, dehydration, paraffin embedding, and sectioning, followed by oven drying. Subsequently, hematoxylin and eosin (H&E) staining and bright field panoramic section scanning were performed.

4.5 Drug release behavior of MNs

Prepare FBP standard solutions at concentrations of 1, 2, 4, 6, and 8 μg/mL using PBS containing 10% ethanol. Use PBS with 10% ethanol as the blank, measure the absorbance of the samples at 247 nm, and construct the standard curve for FBP.

Select a dialysis bag with an appropriate MWCO according to the molecular weight of FBP. Encapsulate the prepared FBP/cGel MNP in the dialysis bag and immerse it in the release medium (PBS containing 10% ethanol), continuously re-leasing it under conditions of 37 °C and 300 rpm. At 10, 20, 30, 60, 90, 120, 180, 240, 300, 360, 480, 600, and 720 min, withdraw 300 μL of the solution and replenish with an equal volume of fresh release medium. Use a microplate reader to measure the absorbance of the sample solutions, subsequently calculating the cumulative drug release rate at respective time points.

4.6 Analgesic efficacy of MNs

Following the methods of Ohri and Duarte et al. [37,43], construct an incisional pain model in the hairy skin of the rat back, using a 10 # scalpel blade to make a longitudinal incision approximately 1.2 cm in length on the skin surface over the L4 transverse process. Bluntly separate the subcutaneous fat and superficial fascia beneath the incision, using the manipulation, skin incision plus extension. After hemostasis, debridement, and dis-infection, suture the wound with two stitches using 3-0 silk thread. Interventions corresponding to each group were administered to rats near the wound site, dividing the ani-mal experiment into five groups: model+blank group (Blank group), model+blank MNP group (cGel MNP), model+FBP HP group (FBP HP), model+FBP/Gel MNP group (FBP/Gel MNP), and model+FBP MNP group (FBP/cGel MNP). Following group allocation and labeling, each rat was placed in a cage to recover from anesthesia. Subsequently, the responses of the rats to mechanical and thermal pain stimuli were evaluated separately.

The method for assessing the response to mechanical pain stimuli is as follows. The skin in different areas on the rats' backs (0.5 cm of the ipsilateral side and the contralateral side of 2 cm) was stimulated at various time points using VFHs (4 g- and 15 g-VFHs, Aesthesio, Danmic, USA), to observe the twitch velocity and amplitude of their CTMR, indicative of nociceptive specificity. Then, the pain sensitization of rats in each group was evaluated, facilitating an evaluation of the therapeutic efficacy of the different intervention measures.

The day before surgery, SD rats were anesthetized via inhalation and the hair on their dorsal skin was removed. This pre-treatment of hair removal resulted in localized irritation to the dorsal skin, which subsided overnight. Preoperatively, the skin at the test sites in rats was repeatedly stimulated with a 4 g-VFH to eliminate the animal's response to non-nociceptive stimuli. According to the method described by Ohri and Duarte et al. [37, 43], each VFH was applied four times at the same spot with equal force, with an interval of 2–3 s between each stimulus. The testing began with the 4 g-VFH and concluded with the 15 g-VFH. According to the response speed and extent of the rat's trunk muscle after each stimulation, the scoring is as follows: no obvious contraction is scored as 0 points, weaker contraction (within 4 cm) is scored as 0.5 points, and stronger contraction (5 cm and above) is scored as 1 point. Finally, the test results are compared in two forms: graded response and population response. The graded response is the weighted average score of the four reaction scores in each trial, with results ranging from 0 to 1. In the population response, any rat that contracts during any trial is marked as 1, while those that do not contract are marked as 0. The result of the population response is the total number of rats marked as "1" in each group divided by the total number of animals in the group, with results ranging from 0 to 100%. This is interpreted as the proportion of animals in each group that respond to punctate mechanical stimuli.

Additionally, the hot-plate test was employed to evaluate the response of each group of rats to thermal pain stimuli. The

temperature of the constant temperature intelligent hot plate apparatus (Beijing Zhongshi Dichuang Technology Development Co. , Ltd.), equipped with a transparent plexiglass cover, was set to a constant temperature of 55 ± 0.2 °C. Once the hot plate reached the set temperature, the plexiglass cover was removed, and the rat was swiftly placed onto the apparatus. The time from when the rat's hind paw made contact with the hot plate until any of the following behaviors occurred—lifting the paw, retracting it, licking it, or struggling—was recorded as the hind paw withdrawal time, also referred to as the PWL. This measurement served as an indicator to assess the rat's thermal pain threshold. The maximum time allowed was set at 30 s (the cut-off value) to prevent scalding of the rat's paw tissue. Each rat was subjected to two repeated measurements, with a 10-min interval between each measurement, and the average value was taken. The thermal pain threshold latency was determined for each rat one day prior to modeling as the baseline thermal pain threshold. Subsequent measurements of the thermal pain threshold were conducted at 0.5, 1, 2, 3, 4, 6, and 8 h post-surgery. The %MPE for each rat was calculated using the following Eq. (2)

$$\% \, MPE = [(LR - BR)/(MR - BR)] \times 100\% \qquad (2)$$

where LR, MR, and BR represent measured, maximum (30 s), and baseline (~ 5 s) response time, respectively.

4.7 Biocompatibility of MNs

The biocompatibility of drug-loaded MNs was evaluated by skin recovery test, cyto-toxicity test, and hemolysis test.

RhB/cGel MNs (RhB, 0.5 w/v%) were applied to the shaven dorsal skin of SD rats for 5 min and then removed. Photographs of the rat skin were taken immediately after MNs removal, and at 1, 2, and 3 h, to observe whether the skin could recover to its normal state and to check for any permanent damage such as infection.

The CCK-8 assay was used to assess cell viability, which serves to evaluate cytotoxicity [44]. In a 96-well plate, 100 μL of L-929 cell suspension was seeded in each well, followed by the addition of 100 μL of appropriate culture medium. Four replicate wells were set up for each group, along with a blank group (culture medium only) and a control group (culture medium + cells + PBS). After seeding, the 96-well plate was placed in a constant temperature incubator. After 24 h, 10 μL of different concentrations of Gel solution, FBP solution, and FBP/cGel MNs extracts were added to their respective wells. The plate was then returned to the constant temperature incubator for 24 h of incubation. After the addition of 10 μL CCK-8 solution, incubate for 3 h. Subsequently, the OD value at 450 nm was measured using a microplate reader. Cell cytotoxicity was calculated using the Eq. (3)

$$Cell \, viability \, (\%) = (A_s - A_o)/(A_c - A_o) \times 100\% \qquad (3)$$

where A_s represents the OD value of the sample well, A_o represents the OD value of the blank well, and A_c represents the OD value of the control well.

Hemolysis tests were conducted to further validate the hemocompatibility of the MNs. Blood was collected from New Zealand rabbits and centrifuged at 1500 rpm for 15 min. The supernatant was discarded, and the red blood cells were washed three times with saline to obtain a red blood cell suspension. Appropriate amounts of the test sample solutions (extracts from cGel MN and FBP/cGel MN), 1 × PBS solution (negative control), and ultrapure water (positive control) were added to the red blood cell suspension. These operations were repeated four times. Samples were gently vortex-mixed, incubated for 1 h, and

centrifuged at 1000 rpm for 5 min. Subsequently, 100 μL of the supernatant from each group was aliquoted into a 96-well plate. The OD at 540 nm was determined using a microplate reader, and the hemolysis rate was calculated using the Eq. (4)

$$Hemolysis \, (\%) = (A_s - A_n)/(A_p - A_n) \times 100\% \qquad (4)$$

where A_s represents the OD value of the sample group, A_n represents the OD value of the negative control group, and A_p represents the OD value of the positive control group.

Concurrently, morphological changes of erythrocytes in each group were observed using an optical microscope.

4.8 Statistical analysis

All analyses were conducted with a sample size of $n \geq 3$. Descriptive statistics were expressed as means values ± SE. The data were analyzed using SPSS 27.0, GraphPad Prism 8.0, and Origin 2022. Differences among three or more groups were analyzed using One-way ANOVA, with pairwise comparisons performed for multiple comparisons. Differences were considered statistically significant at $P < 0.05$.

Electronic Supplementary Material: Supplementary material (Fig. S1: schematic diagram of molecular level of the crosslinking principle of genipin-crosslinked gelatin; Fig. S2: color change of cGel solution with crosslinking time; Fig. S3: morphology of the fabricated FBP/Gel MNs imaged by macro camera (a) and optical microscopy (b); Fig. S4: morphological changes experienced by the FBP/cGel MNs before (a) and after (b) the axial force test. Fig. S5: the molecular structure of flurbiprofen (a) and its standard curve (b); Fig. S6: analgesic efficacy study (n = 5). Population response of primary (a) and secondary (b) allodynia) is available in the online version of this article at https://doi.org/10.1007/s12274-024-6751-x.

References

[1] Taylor, R. S.; Ullrich, K.; Regan, S.; Broussard, C.; Schwenkglenks, M.; Taylor, R. J.; Gordon, D. B.; Zaslansky, R.; Meissner, W.; Rothaug, J. et al. The impact of early postoperative pain on health-related quality of life. *Pain Pract.* **2013**, *13*, 515–523.

[2] Mitra, S.; Carlyle, D.; Kodumudi, G.; Kodumudi, V.; Vadivelu, N. New advances in acute postoperative pain management. *Curr. Pain Headache Rep.* **2018**, *22*, 35.

[3] Benyamin, R.; Trescot, A. M.; Datta, S.; Buenaventura, R.; Adlaka, R.; Sehgal, N.; Glaser, S. E.; Vallejo, R. Opioid complications and side effects. *Pain Physician* **2008**, *11*, S105–S120.

[4] Joshi, G. P.; Kehlet, H. Postoperative pain management in the era of ERAS: An overview. *Best Pract. Res. Clin. Anaesthesiol.* **2019**, *33*, 259–267.

[5] O'Neill, A.; Lirk, P. Multimodal analgesia. *Anesthesiol. Clin.* **2022**, *40*, 455–468.

[6] Schug, S. A.; Manopas, A. Update on the role of non-opioids for postoperative pain treatment. *Best Pract. Res. Clin. Anaesthesiol.* **2007**, *21*, 15–30.

[7] Gustafsson, U. O.; Scott, M. J.; Hubner, M.; Nygren, J.; Demartines, N.; Francis, N.; Rockall, T. A.; Young-Fadok, T. M.; Hill, A. G.; Soop, M. et al. Guidelines for perioperative care in elective colorectal surgery: Enhanced Recovery After Surgery (ERAS®) Society recommendations: 2018. *World J. Surg.* **2019**, *43*, 659–695.

[8] Cashman, J. N. The mechanisms of action of NSAIDs in analgesia. *Drugs* **1996**, *52*, 13–23.

[9] Gupta, A.; Bah, M. NSAIDs in the treatment of postoperative pain. *Curr. Pain Headache Rep.* **2016**, *20*, 62.

[10] Nathi, R.; Ketha, N. V. D. P.; Kowtarapu, L. P.; Muchakayala, S. K.; Konduru, N.; Saroja, B.; Marisetti, A. L. Flurbiprofen cataplasms: Development and validation of *in-vitro* dissolution methods and evaluation of multimedia dissolution profiles. *Pharm. Sci. Adv.* **2023**, *1*, 100018.

[11] Shah, K.; Gupta, J. K.; Chauhan, N. S.; Upmanyu, N.; Shrivastava, S. K.; Mishra, P. Prodrugs of NSAIDs: A review. *Open Med. Chem. J.* **2017**, *11*, 146–195.

[12] Nir, Y.; Paz, A.; Sabo, E.; Potasman, I. Fear of injections in young adults: Prevalence and associations. *Am. J. Trop. Med. Hyg.* **2003**, *68*, 341–344.

[13] Usach, I.; Martinez, R.; Festini, T.; Peris, J. E. Subcutaneous injection of drugs: Literature review of factors influencing pain sensation at the injection site. *Adv. Ther.* **2019**, *36*, 2986–2996.

[14] Prausnitz, M. R.; Langer, R. Transdermal drug delivery. *Nat. Biotechnol.* **2008**, *26*, 1261–1268.

[15] Jiang, J. Z.; Ma, T. Y.; Zhang, L. H.; Cheng, X. M.; Wang, C. H. The transdermal performance, pharmacokinetics, and anti-inflammatory pharmacodynamics evaluation of harmine-loaded ethosomes. *Drug Dev. Ind. Pharm.* **2020**, *46*, 101–108.

[16] Yu, Y. Q.; Yang, X.; Wu, X. F.; Fan, Y. B. Enhancing permeation of drug molecules across the skin via delivery in nanocarriers: Novel strategies for effective transdermal applications. *Front. Bioeng. Biotechnol.* **2021**, *9*, 646554.

[17] An, H.; Gu, Z.; Huang, Z.; Huo, T.; Xu, Y. X.; Dong, Y. Z.; Wen, Y. Q. Novel microneedle platforms for the treatment of wounds by drug delivery: A review. *Colloids Surf. B Biointerfaces* **2024**, *233*, 113636.

[18] Zheng, M. J.; Sheng, T.; Yu, J. C.; Gu, Z.; Xu, C. J. Microneedle biomedical devices. *Nat. Rev. Bioeng.* **2024**, *2*, 324–342.

[19] Nordquist, L.; Roxhed, N.; Griss, P.; Stemme, G. Novel microneedle patches for active insulin delivery are efficient in maintaining glycaemic control: An initial comparison with subcutaneous administration. *Pharm. Res.* **2007**, *24*, 1381–1388.

[20] Van Der Maaden, K.; Jiskoot, W.; Bouwstra, J. Microneedle technologies for (trans) dermal drug and vaccine delivery. *J. Controlled Release* **2012**, *161*, 645–655.

[21] Omatsu, T.; Chujo, K.; Miyamoto, K.; Okida, M.; Nakamura, K.; Aoki, N.; Morita, R. Metal microneedle fabrication using twisted light with spin. *Opt. Express* **2010**, *18*, 17967–17973.

[22] Chen, B. T.; Wei, J. S.; Tay, F. E. H.; Wong, Y. T.; Iliescu, C. Silicon microneedle array with biodegradable tips for transdermal drug delivery. *Microsyst. Technol.* **2008**, *14*, 1015–1019.

[23] Ita, K. Ceramic microneedles and hollow microneedles for transdermal drug delivery: Two decades of research. *J. Drug Deliv. Sci. Technol.* **2018**, *44*, 314–322.

[24] Han, J. P.; Sheng, T.; Zhang, Y. Q.; Cheng, H.; Gao, J. Q.; Yu, J. C.; Gu, Z. Bioresponsive immunotherapeutic materials. *Adv. Mater.*, in press, https://doi.org/10.1002/adma.202209778.

[25] Yang, Y.; Chu, H. Q.; Zhang, Y.; Xu, L. L.; Luo, R. Z.; Zheng, H.; Yin, T. L.; Li, Z. Rapidly separable bubble microneedle patch for effective local anesthesia. *Nano Res.* **2022**, *15*, 8336–8344.

[26] Luo, F. Q.; Chen, G. J.; Xu, W.; Zhou, D. J.; Li, J. X.; Huang, Y. C.; Lin, R.; Gu, Z.; Du, J. Z. Microneedle-array patch with pH-sensitive

[27] Hong, T.; Shen, X. Y.; Syeda, M. Z.; Zhang, Y.; Sheng, H. N.; Zhou, Y. P.; Xu, J. M.; Zhu, C. J.; Li, H. J.; Gu, Z. et al. Recent advances of bioresponsive polymeric nanomedicine for cancer therapy. *Nano Res.* **2023**, *16*, 2660–2671.

[28] Su, K.; Wang, C. M. Recent advances in the use of gelatin in biomedical research. *Biotechnol. Lett.* **2015**, *37*, 2139–2145.

[29] Echave, M. C.; Hernáez-Moya, R.; Iturriaga, L.; Pedraz, J. L.; Lakshminarayanan, R.; Dolatshahi-Pirouz, A.; Taebnia, N.; Orive, G. Recent advances in gelatin-based therapeutics. *Expert Opin. Biol. Ther.* **2019**, *19*, 773–779.

[30] Liang, H. C.; Chang, W. H.; Liang, H. F.; Lee, M. H.; Sung, H. W. Crosslinking structures of gelatin hydrogels crosslinked with genipin or a water-soluble carbodiimide. *J. Appl. Polym. Sci.* **2004**, *91*, 4017–4026.

[31] Bozzini, S.; Petrini, P.; Altomare, L.; Tanzi, M. C. Fabrication of chemically cross-linked porous gelatin matrices. *J. Appl. Biomater. Biomech.* **2009**, *7*, 194–199.

[32] Vijayakumar, V.; Subramanian, K. Diisocyanate mediated polyether modified gelatin drug carrier for controlled release. *Saudi Pharm. J.* **2014**, *22*, 43–51.

[33] Ahmed, R.; Ul Ain Hira, N.; Wang, M. W.; Iqbal, S.; Yi, J.; Hemar, Y. Genipin, a natural blue colorant precursor: Source, extraction, properties, and applications. *Food Chem.* **2024**, *434*, 137498.

[34] Kirchmajer, D. M.; Watson, C. A.; Ranson, M.; Panhuis, M. I. H. Gelapin, a degradable genipin cross-linked gelatin hydrogel. *RSC Adv.* **2013**, *3*, 1073–1081.

[35] Butler, M. F.; Ng, Y. F.; Pudney, P. D. A. Mechanism and kinetics of the crosslinking reaction between biopolymers containing primary amine groups and genipin. *J. Polym. Sci. A Pol. Chem.* **2003**, *41*, 3941–3953.

[36] Bigi, A.; Panzavolta, S.; Roveri, N. Hydroxyapatite-gelatin films: A structural and mechanical characterization. *Biomaterials* **1998**, *19*, 739–744.

[37] Ohri, R.; Wang, J. C. F.; Blaskovich, P. D.; Pham, L. N.; Costa, D. S.; Nichols, G. A.; Hildebrand, W. P.; Scarborough, N. L.; Herman, C. J.; Strichartz, G. R. Inhibition by local bupivacaine-releasing microspheres of acute postoperative pain from hairy skin incision. *Anesth. Analg.* **2013**, *117*, 717–730.

[38] Van De Loosdrecht, A. A.; Nennie, E.; Ossenkoppele, G. J.; Beelen, R. H. J.; Langenhuijsen, M. M. A. C. Cell mediated cytotoxicity against U 937 cells by human monocytes and macrophages in a modified colorimetric MTT assay: A methodological study. *J. Immunol. Methods* **1991**, *141*, 15–22.

[39] Zhen, Z.; Liu, X. L.; Huang, T.; Xi, T. F.; Zheng, Y. F. Hemolysis and cytotoxicity mechanisms of biodegradable magnesium and its alloys. *Mater. Sci. Eng. C* **2015**, *46*, 202–206.

[40] Chen, B. Z.; Zhang, L. Q.; Xia, Y. Y.; Zhang, X. P.; Guo, X. D. A basal-bolus insulin regimen integrated microneedle patch for intraday postprandial glucose control. *Sci. Adv.* **2020**, *6*, eaba7260.

[41] Friedman, M. Applications of the ninhydrin reaction for analysis of amino acids, peptides, and proteins to agricultural and biomedical sciences. *J. Agric. Food Chem.* **2004**, *52*, 385–406.

[42] Wang, Q. L.; Zhu, D. D.; Chen, Y.; Guo, X. D. A fabrication method of microneedle molds with controlled microstructures. *Mater. Sci. Eng. C* **2016**, *65*, 135–142.

[43] Duarte, A. M.; Pospisilova, E.; Reilly, E.; Mujenda, F.; Hamaya, Y.; Strichartz, G. R. Reduction of postincisional allodynia by subcutaneous bupivacaine: Findings with a new model in the hairy skin of the rat. *Anesthesiology* **2005**, *103*, 113–125.

[44] Podgórski, R.; Wojasiński, M.; Ciach, T. Nanofibrous materials affect the reaction of cytotoxicity assays. *Sci. Rep.* **2022**, *12*, 9047.

formulation for glucose-responsive insulin delivery. *Nano Res.* **2021**, *14*, 2689–2696.